Impact of high-order moments on the statistical modeling of transition arrays

Franck Gilleron* and Jean-Christophe Pain
CEA/DIF, B.P. 12, 91680 Bruyères-Le-Châtel Cedex, France

Jacques Bauche and Claire Bauche-Arnoult
Laboratoire Aimé Cotton, CNRS II, Bâtiment 505, 91405 Orsay, France
(Received 8 November 2007; published 27 February 2008)

The impact of high-order moments on the statistical modeling of transition arrays in complex spectra is studied. It is shown that a departure from the Gaussian, which is usually employed in such an approach, may be observed even in the shape of unresolved spectra due to the large value of the kurtosis coefficient. The use of a Gaussian shape may also overestimate the width of the spectra in some cases. Therefore, it is proposed to simulate the statistical shape of the transition arrays by the more flexible generalized Gaussian distribution which introduces an additional parameter—the power of the argument in the exponential—that can be constrained by the kurtosis value. The relevance of the statistical line distribution is checked by comparisons with smoothed spectra obtained from detailed line-by-line calculations. The departure from the Gaussian is also confirmed through the analysis of $2p$-$3d$ transitions of recent absorption measurements. A numerical fit is proposed for an easy implementation of the statistical profile in atomic-structure codes.

DOI: 10.1103/PhysRevE.77.026708 PACS number(s): 05.10.−a, 32.70.−n, 52.25.Os

I. INTRODUCTION

The computation of detailed-line spectra is often a challenging—if not impossible—task for high-Z plasmas, due to the large amount of levels and lines involved. The good side of this complexity is that lines can merge into simple broad structures. This allows one to use global methods in which atomic properties of ions are averaged in some ways. In this work, we focus our attention on the statistical approach which uses the moments of the line distributions to build the spectra of complex ions. This can be done, for example, by using the Gram-Charlier expansion series which allows one to account for an arbitrary number of moments [1,2]. In fact, many similar developments exist, based on orthogonal polynomials, continuous fractions, Fourier series, etc. A major consequence of information theory is that the more complex the spectrum is, the larger is the number of moments required for a good depiction. The convergence of the development in moments may also be an issue.

The principal interest of the statistical approach in atomic spectroscopy resides in the ability to provide compact formulas for the moments, bypassing thus the construction and the diagonalization of the Hamiltonian of the system. The moments of any transition array have been derived analytically by Bauche-Arnoult *et al.* [3] as functions of radial integrals, but only up to the second order. Compact formulas have been published by the same authors for the third-order moment [4], but they are incomplete and can be used only for certain types of transition array. Parts of the fourth-order moment have been derived also by Karazija [5], using graphical methods. Therefore, the statistical approach can be used only to represent unresolved transition arrays (UTA). The term "unresolved" means that it is not possible to locate any feature associated to a particular level-to-level transition. This is due to the high density of levels and lines that arises when high-Z configurations with one or more open shells of high degeneracy are considered. This occurs also if the individual linewidth, due to physical broadening mechanisms, is sufficiently large to smooth the transition array. It is important to mention that there is no simple way to determine whether a transition array is resolved or unresolved without performing the exact line-by-line calculation. Despite the use of coarse criterions regarding the ion density or the atomic number, the UTA approach is often used blindly.

The main issue addressed in this paper is the choice of the relevant distribution for modeling the unresolved transition arrays. Though it is quite convenient to employ a Gaussian function knowing the first two moments of the distribution, this choice remains arbitrary and is not imposed by the UTA approach. Indeed, from a mathematical point of view, many distributions can be built from the known low-order moments, and physical arguments are strongly needed to guide the most relevant choice. The use of a Gaussian for the statistical modeling of transition arrays owes most of its popularity to the success of the random matrix theory [6] in various fields, especially for simulating the complex spectra in nuclear physics [7]. Attempts to use the properties of the Gaussian orthogonal ensemble (GOE) in atomic physics [8], and empirical studies [9] of wavelength and oscillator-strength distributions have shown that things could be more complicated. For example, it is well known that correlations exist between the line energies and their amplitudes [10]. Such effects are obvious by considering that, as a general trend, the strongest lines are found closer to the center of gravity than the weakest lines, and that the variance of the line energies is always smaller when it is calculated with a weight equal to the line strength than when it is not. The transition arrays of the type $\ell^N\ell'$-$\ell^N\ell''$ are good examples of this phenomenon, because of the fierce selection rules on the core ℓ^N. They are known to be much sharper than a Gaussian distribution.

*franck.gilleron@cea.fr

 ©2008 The American Physical Society

Throughout the paper, emphasis is put on the effects of the kurtosis coefficient on symmetrical line distributions. Accounting for the skewness factor seems to be a less critical issue. Indeed, highly asymmetrical line distributions can be found either close to the *LS* coupling, due to a large G^1 Slater integral [11], or in situations where the spin-orbit interactions are strong enough to initiate the splitting of the transition array. In the latter case, which is more frequent for medium- or high-Z elements, the asymmetrical shape of the array can be restored by considering the superposition of symmetrical subarrays based on relativistic [12] or semirelativistic [13] configurations. However, effects of the electrostatic operator on levels of (semi-)relativistic configurations must be taken into account carefully, as they can strongly alter the intensity of each subarray [13,14].

In Sec. II, the transition arrays are defined and the main approximations of the UTA model are recalled. In Sec. III, the choice between a Gaussian function, truncated Gram-Charlier series, or generalized Gaussian function to simulate the statistical line distributions is then discussed by studying the high-order moments. The effects of the linewidth and of the spin-orbit interactions are also tackled. In Sec. IV, a numerical fit of the generalized Gaussian functions is proposed for an easy implementation in atomic-structure codes. Finally, the profile is used to study the non-Gaussian effects in some recent experiments.

II. UNRESOLVED TRANSITION ARRAYS MODEL

Transition arrays are spectroscopical objects characterized by specific distributions of photon energy E,

$$I(E) = C_p \sum_{ab} \frac{N_a}{g_a} (E_{ab})^p S_{ab} \Psi(E - E_{ab}), \tag{1}$$

which, using the appropriate constant factor C_p, represent either the opacity coefficient ($p=1$), the number of emitted photons ($p=3$), or the emissivity of the source ($p=4$). The sum runs over the upper and lower levels of each line belonging to the transition array. The density of level a is noted N_a, and its degeneracy g_a. The energy of the line $a \rightarrow b$ is $E_{ab}=E_a-E_b$, the line strength is S_{ab}, and $\Psi(E-E_{ab})$ is a normalized profile that takes into account the broadening of the line in the plasma by the various external processes (natural width, Doppler, Stark, electron collisions, etc.).

The distribution $I(E)$ can be expressed equivalently as a convolution product,

$$I(E) = A(E) \otimes \Psi(E), \tag{2}$$

where the function $A(E)$ assumes that each line is represented by a Dirac δ function,

$$A(E) = C_p \sum_{ab} \frac{N_a}{g_a} (E_{ab})^p S_{ab} \delta(E - E_{ab}). \tag{3}$$

The usual UTA modeling is based on the following three approximations:

Assumption 1. The discrete distribution $A(E)$ can be replaced by a continuous distribution (usually Gaussian or skewed Gaussian) which preserves its low-order moments.

Assumption 2. Under the assumption of statistical weight population, the density N_a of level a is assumed to be proportional to its statistical weight g_a,

$$\frac{N_a}{g_a} \approx \frac{N_0}{g_0}, \tag{4}$$

with $N_0=\Sigma_a N_a$ and $g_0=\Sigma_a g_a$.

Assumption 3. In order to avoid the sum over the term $(E_{ab})^p$ in Eq. (3), the line energy E_{ab} is replaced by the center of gravity E_0 of the transition array,

$$(E_{ab})^p \approx (E_0)^p. \tag{5}$$

The last two assumptions allow one to express $A(E)$ in the form

$$A(E) \approx C_p \frac{N_0}{g_0} (E_0)^p \sum_{ab} S_{ab} \delta(E - E_{ab}) \tag{6}$$

and the moments of this distribution as

$$\mu_n(A) = \frac{\int_{-\infty}^{\infty} A(E) E^n dE}{\int_{-\infty}^{\infty} A(E) dE} \approx \frac{\sum_{ab} S_{ab} (E_{ab})^n}{\sum_{ab} S_{ab}}. \tag{7}$$

With these assumptions, it is possible to derive analytical formulas for the moments $\mu_n(A)$ using the quantum-mechanical algebra of Racah and second-quantization techniques of Judd [15]. Such expressions, which depend only on radial integrals, have been published by Bauche-Arnoult and co-workers [3,4,12,16] for the moments μ_n (with $n \leqslant 3$) of several kinds of transition arrays (relativistic or not). First-order corrections have been proposed by the same authors [17] to account for a Maxwell-Boltzmann population factor (second assumption). It can be shown that the third assumption amounts to neglecting powers of σ/μ_1 [with $\sigma^2=\mu_2-(\mu_1)^2$] in the exact expression of the moments. The case of opacity ($p=1$) is discussed in the Appendix. However, the choice of a Gaussian or skewed Gaussian distribution (first assumption) does not play any role for the derivation of the moments. It is only used to substitute for the discrete line distribution $A(E)$ in Eq. (2). This will be discussed in the next section.

III. STUDY OF THE RECONSTRUCTED LINE DISTRIBUTIONS

A. Definitions

Throughout the paper, it is assumed that all the moments of the distribution $A(E)$ exist. For the modeling of transition arrays, it is useful to introduce the reduced centered moments of the distribution defined by

$$\alpha_n(A) = \frac{1}{\Omega} \int_{-\infty}^{\infty} A(E) \left(\frac{E - \mu_1}{\sigma} \right)^n dE \tag{8}$$

$$= \frac{1}{\sigma^n} \sum_{i=0}^{n} \binom{n}{i} \mu_i (-\mu_1)^{n-i}, \tag{9}$$

where μ_1 is the center of gravity of the strength-weighted line energies, $\sigma = \sqrt{\mu_2 - \mu_1^2}$ is the standard deviation, and $\Omega = \int_{-\infty}^{\infty} A(E)dE$ is the total area of the distribution. The use of $\alpha_n(A)$ instead of $\mu_n(A)$ allows one to deal with more reasonable numbers, limiting that way the numerical problems. The first values $\alpha_0 = 1$, $\alpha_1 = 0$, and $\alpha_2 = 1$ are trivial by definition. The distribution $A(E)$ is therefore fully characterized by the values of Ω, μ_1, σ and by the values of the high-order moments α_n with $n > 2$.

The third- and fourth-order reduced centered moments α_3 and α_4 are the well-known *skewness* and *kurtosis* coefficients, respectively. A non-null value of the former allows one to quantify the asymmetry of the distribution. The latter is a measure of the flattening of the distribution at the center; it is usually compared to the value $\alpha_4 = 3$ for a Gaussian distribution.

B. Gram-Charlier expansion series

An analytical function which preserves an arbitrary number of moments can be built using the properties of orthogonal polynomials and their associated basis functions [1]. The type-*A* Gram-Charlier (GC) expansion series is a combination of products of Hermite polynomials by a Gaussian function,

$$H_n(E) = \frac{\Omega}{\sigma} \frac{e^{-u^2/2}}{\sqrt{2\pi}} \left(1 + \sum_{k=2}^{n} c_k \, \mathrm{He}_k(u) \right) \tag{10}$$

with

$$c_k = \sum_{j=0}^{\mathrm{int}(k/2)} \frac{(-1)^j}{j!\,(k-2j)!\,2^j} \alpha_{k-2j}(A), \tag{11}$$

where $u = (E - \mu_1)/\sigma$, n is the number of moments, $\mathrm{He}_k(u)$ is the Hermite polynomial of order k, and $\mathrm{int}(k/2)$ is the integer part of $k/2$. The GC series uses the reduced centered moments $\alpha_k(A)$ of the discrete distribution $A(E)$. When carried on to infinity, it can be shown that the GC expansion series is an exact representation of the distribution: $A(E) = \lim_{n\to\infty} H_n(E)$. The truncated series $H_n(E)$ may be viewed as a Gaussian function multiplied by a polynomial which accounts for the effects of departure from normality. Therefore it may be a slowly converging series when $A(E)$ differs strongly from the Gaussian distribution. This is illustrated in Fig. 1, where it can be seen that at least 50 moments are needed to reproduce the shape of the transition array $3d^6$-$3d^5 4p$ in Br^{11+}. Moreover, the truncating has the drawback of yielding negative values in some circumstances. It is also known to suffer from numerical instability since Eq. (11) involves a sum of large terms of alternating sign.

C. Fourth-order moment distributions

The main properties of a bell-shaped distribution can be captured by its first four moments, which represent qualitatively the center of gravity, the width, the asymmetry, and the sharpness of the distribution. This can be checked in Fig. 1 by noticing that the GC series does not change much between the orders 4 and 10.

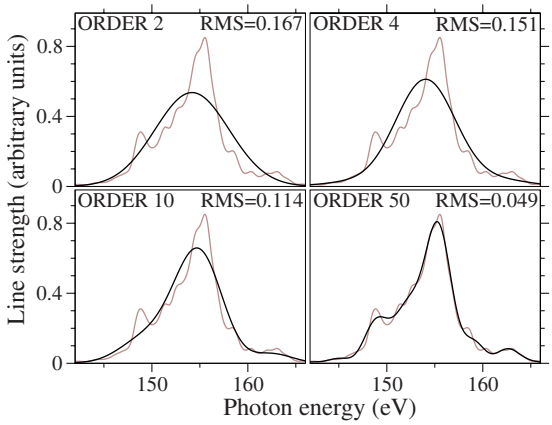

FIG. 1. (Color online) Convergence of the Gram-Charlier expansion series for the array $3d^6$-$3d^5 4p$ in bromine. The heavy line is a representation of the distribution $A(E)$ using a GC series up to a specified order. The light curve is an exact calculation performed with Cowan's code [9] and smoothed with a resolution $\lambda/\delta\lambda = 150$ to make easier the comparison with GC. The relative root mean square (RMS), given in upper right corner on the figures, is a measure of the squared distance between both distributions.

In the following, the emphasis is put on the study of the impact of the kurtosis coefficient in a symmetrical distribution ($\alpha_3 = 0$). Many distributions preserving the four parameters (Ω, μ_1, σ, and α_4) can still be found. A noncomprehensive list includes the following: Gram-Charlier series, normal inverse Gaussian, Student's, Pearson's, and Γ and generalized Gaussian distributions. Our goal is not so much to determine which specification seems to be the most accurate as to find a distribution which allows one to study easily the effects of the departure from the Gaussian law (including the normal law as a particular case). First, let us consider the fourth-order GC series,

$$H_4(E) = \frac{\Omega}{\sigma} \frac{e^{-u^2/2}}{\sqrt{2\pi}} \left(1 + \frac{(\alpha_4 - 3)}{24} (3 - 6u^2 + u^4) \right). \tag{12}$$

This distribution is presented in Fig. 2 for various values of α_4. The main drawbacks are the negative signs for $\alpha_4 > 7$, and the presence of nonphysical bumps on the tail on either side of the distribution.

It seems to us that the best choice to study the effects of the kurtosis is the generalized Gaussian distribution (GG), defined by

$$P(E) = \frac{\Omega}{\sigma} \frac{e^{-|u/\lambda|^\nu}}{2\lambda\Gamma\left(1 + \frac{1}{\nu}\right)}, \quad \text{with } \lambda = \sqrt{\frac{\Gamma\left(\frac{1}{\nu}\right)}{\Gamma\left(\frac{3}{\nu}\right)}}, \tag{13}$$

where ν is a positive real number and $\Gamma(x)$ is the ordinary gamma function. The even-order moments of a GG function read

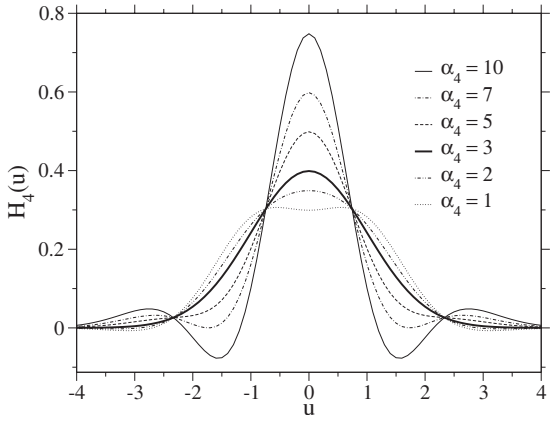

FIG. 2. Fourth-order symmetrical Gram-Charlier distributions for several values of the kurtosis coefficient α_4. The thick line corresponds to a Gaussian function.

$$\alpha_{2k}(P) = \lambda^{2k} \frac{\Gamma\left(\frac{1+2k}{\nu}\right)}{\Gamma\left(\frac{1}{\nu}\right)}, \tag{14}$$

whereas the odd-order moments are null, $\alpha_{2k+1}(P)=0$, because of the symmetry. The parameter ν can be obtained by constraining the kurtosis coefficient, and thus solving the equation

$$\ln \alpha_4 = \ln \Gamma(1/\nu) + \ln \Gamma(5/\nu) - 2 \ln \Gamma(3/\nu). \tag{15}$$

This distribution can be observed in Fig. 3 for several values of the parameter ν. The GG function has interesting properties. It is a simple increasing (decreasing) function for $u>0$ $(u<0)$, without weird features as in GC series. The Gaussian $(\nu=2)$ and the Laplace $(\nu=1)$ distributions are special cases of GG functions with a kurtosis coefficient equal to 3 and 6, respectively. Asymptotically, the GG function tends to a square function with $\alpha_4=9/5$ for $\nu\to\infty$, and to a Dirac δ function for $\nu\to 0$. The GG functions with $0<\nu\leqslant 1$ have a nondefinite derivative at $u=0$, but this discontinuity disappears with the convolution by another function, as in Eq. (2).

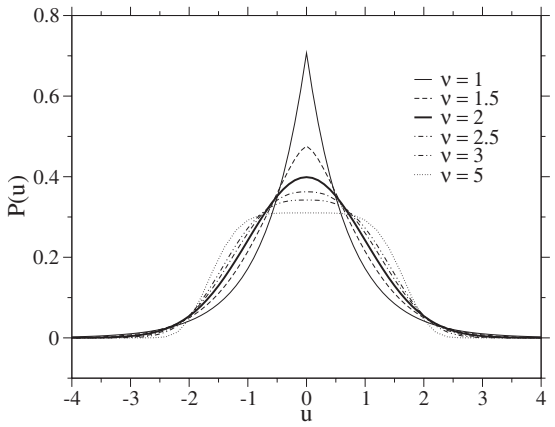

FIG. 3. Generalized Gaussian distributions for several values of the parameter ν. The thick line corresponds to a Gaussian function.

TABLE I. Values of the even reduced centered moments α_k of several distributions representing the transition array $3d^6$-$3d^5 4p$ in bromine. Exact: calculation with Cowan's code; $P(E)$: generalized Gaussian function with $\nu=1.356$; $H_4(E)$: fourth-order Gram-Charlier series with $\alpha_3=0$ and $\alpha_4=4.1481$.

Order	Exact	$P(E)$	$H_4(E)$	Gaussian
4	4.1481	4.1481	4.1481	3
6	33.589	34.730	32.222	15
8	433.98	466.46	346.10	105
10	7771.7	8953.6	4561.6	945
12	1.73×10^5	2.29×10^5	0.70×10^5	10395
14	4.52×10^6	7.45×10^6	1.22×10^6	135140

The full width at half maximum (FWHM) of a GG function is given by the formula

$$X_{\mathrm{FWHM}}(P) = 2\sigma\lambda(\ln 2)^{1/\nu}. \tag{16}$$

It is worth mentioning that the conservation of the variance does not imply the conservation of the FWHM. The latter quantity depends obviously of the distribution itself. For example, the above formula gives $X_{\mathrm{FWHM}}=2.35\sigma$ for a Gaussian $(\nu=2)$ and $X_{\mathrm{FWHM}}=0.98\sigma$ for a Laplace distribution $(\nu=1)$.

D. Influence of the higher moments

The choice of a specific distribution with some constraints over low-order moments of the discrete distribution $A(E)$ fixes *ipso facto* the higher unconstrained moments. This can be seen in Table I, for the transition array $3d^6$-$3d^5 4p$ in bromine, which shows the values of the even reduced centered moments α_k up to the order 14 for several distributions. The exact values of the moments are calculated with Cowan's code [9]. They are compared with the values of the GG function, using Eq. (14), and with the values of the fourth-order GC series, obtained by setting $c_k=0$ for $k\geq 6$. Both functions $P(E)$ and $H_4(E)$ are constrained by the moments of order $k\leq 4$ of the exact distribution. Values for the Gaussian function are also shown. It is observed, for this particular case, that the GG function is slightly closer to the exact values than the fourth-order GC series. One concludes also that the Gaussian distribution is not a good representation for that array. This can be checked also in Figs. 5(a)–5(c) by noticing the large discrepancies between the Gaussian and the exact line-by-line calculation.

It is interesting to study the other type of transition array, $\ell^N\ell'$-$\ell^N\ell''$, which is known to be very narrow due to the strong selection rules on the core ℓ^N. As an example, Table II shows the case $3d^5 4s$-$3d^5 4p$ in bromine. As expected, this is a difficult case since the kurtosis is equal to 14.194, and the values of successive even moments of the exact distribution increase very rapidly. The GC series is useless here due to the occurrence of negative signs. A GG function which preserves the kurtosis value is obtained for $\nu=0.624$. However, it seems that a parameter ν between 0.7 and 0.8 would be a better choice, since it allows one to reproduce as an average the higher moments up to the order 14.

TABLE II. Same as Table I for $3d^5 4s$-$3d^5 4p$ in bromine. Here, the exact values of the higher moments are compared with the values deduced from several GG functions. The GC series is useless here due to the occurrence of negative signs.

		$P(E)$		
Order	Exact	$\nu=0.624$	$\nu=0.701$	$\nu=0.797$
4	14.194	14.194	11.014	8.6183
6	589.14	824.68	429.65	228.62
8	40009	126670	40009	13113
10	3.72×10^6	4.09×10^7	7.24×10^6	1.35×10^6
12	4.25×10^8	2.42×10^{10}	2.25×10^9	2.25×10^8
14	5.58×10^{10}	2.37×10^{13}	1.09×10^{12}	5.58×10^{10}

E. Line broadening effects

The preceding section was devoted to the study of the discrete line distribution $A(E)$ and to the relevance of the Gaussian or the GG functions as a suitable representation. But one has to keep in mind that the quantity which is measured during an experiment is $I(E)$. Equation (2) shows that this spectrum is dependent on the interplay of the individual line profile $\Psi(E)$ and of the discrete line distribution $A(E)$. Therefore, another way to test the analytical representation of the UTA is to analyze how the spectrum $I(E)$ changes from a detailed shape to an unresolved structure due to the individual line broadening.

For this test, the broadening $\Psi(E)$ is simply replaced by a Gaussian profile. Figures 4 and 5 show the evolution of the reconstructed spectra $I(E)$, for two types of transition arrays, as a function of the width of the Gaussian profile Δ. The transition array $3d^5 4s$-$3d^5 4p$ of bromine is presented in Fig.

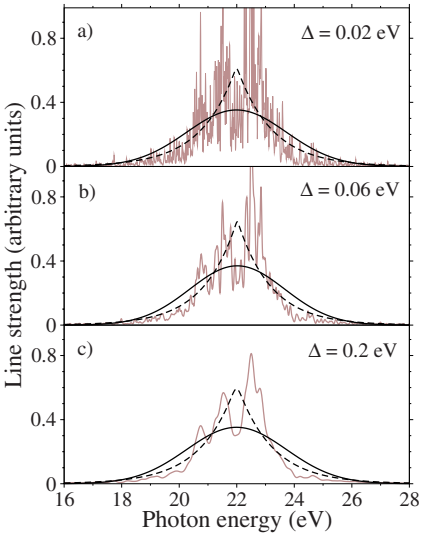

FIG. 4. (Color online) Effects of the convolution linewidth Δ on the line distributions of Br^{11+} $3d^5 4s$-$3d^5 4p$. The detailed-line calculations (light curve) are performed using Cowan's code. The Gaussian distributions (heavy line) and the GG distributions with $\nu=1$ (dashed line) are constrained by the low-order moments $k\leq 2$.

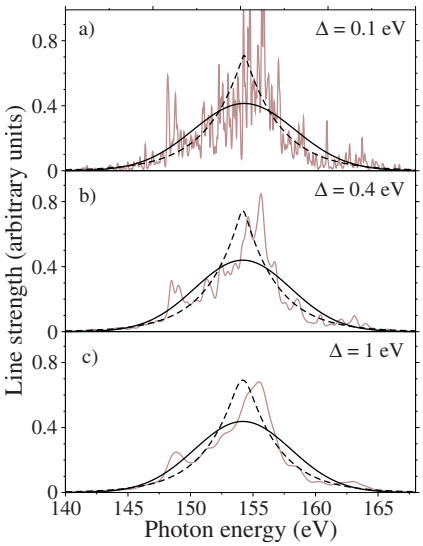

FIG. 5. (Color online) Same as Fig. 4 for Br^{11+} $3d^6$-$3d^5 4p$.

4. Cowan's code gives the following informations: 7426 lines, $\mu_1=22.016$ eV, $\sigma=1.65$ eV, $\alpha_3=-0.108$, and $\alpha_4=14.194$. The transition array $3d^6$-$3d^5 4p$ of bromine, shown in Fig. 5, contains 3245 lines, and is characterized by the following moments: $\mu_1=154.18$ eV, $\sigma=3.84$ eV, $\alpha_3=0.123$, and $\alpha_4=4.148$.

The statistical calculations, based on a Gaussian or a GG function, are compared with the exact spectrum obtained from Cowan's code. In both examples, the same GG function with $\nu=1$ is used. This represents roughly the mean value of the optimized parameters ν that has been found in the last section ($\nu=0.8$ and $\nu=1.356$) for these arrays. This allows one, also, to see the sensitivity with respect to ν of a reconstructed spectrum based on a GG function.

Figures 4 and 5 show that the GG function with $\nu=1$ is in better agreement with the exact calculations considering the width and the height of the distributions. It is also more satisfactory for the tails of these spectra which show an exponential-like behavior clearly not Gaussian. In Figs. 4(a) and 5(a), it is difficult to visually discriminate between the GG and Gaussian distributions, because the spectra become too much resolved. But this corresponds to situations where, by definition, the unresolved transition array model is not well suited. Anyway, it is possible to quantify roughly the similarity of the GG function with respect to the exact profile by computing the root mean square (rms) distance between both curves. The results, presented in Table III, show that the GG function with $\nu=1$ is always closer to the exact profile than with $\nu=2$, though the differences between both values of ν become more tenuous and the gap from the exact curve larger as Δ decreases.

F. Spin-orbit effects

More generally, the frequency-dependent shape of a transition array depends also on the relative importance of the electrostatic and spin-orbit effects. The latter become predominant when the atomic number Z increases. The reason is that, for the same isoelectronic sequence, the matrix ele-

TABLE III. Values of the root mean square RMS distance (in unit of 10^{-3} of the total area) between the exact profile and a GG distribution ($\nu=1$ or 2), as a function of the assumed Gaussian linewidth. The cases considered are those of Figs. 4 and 5.

Transition arrays in Figs. 4 and 5	Gaussian linewidth Δ (in eV)	rms $\nu=1$	rms $\nu=2$
$3d^5 4s$-$3d^5 4p$	0.2	26.57	28.83
	0.06	33.86	35.28
	0.02	45.36	46.40
$3d^6$-$3d^5 4p$	1	9.39	10.20
	0.4	11.65	12.11
	0.1	17.48	17.78

ments of the Coulomb and spin-orbit operators are proportional to Z and Z^4, respectively. As a consequence, the transition arrays may split into two or three relativistic structures for a high-Z element. The statistical properties of each subarray can be obtained with an intermediate coupling model based on a fully or semirelativistic-configuration description, including corrections for the configuration interaction effects [12–14].

Because a Gaussian function is wider and decreases more rapidly in the tail than a GG function with $\nu<2$, the overlapping range between two nearby structures is a good test for the relevance of the statistical profiles. This can be observed in Fig. 6 which shows the evolution of the isoelectronic sequence $3d^5$-$3d^4 4p$ as a function of the atomic number. In the case $Z=68$, it can be noticed that the spectral range between both subarrays is better reproduced with Laplace (GG function with $\nu=1$) than with Gaussian distributions. In all cases, the use of Laplace distributions leads to a remarkable agreement with the exact calculations, especially for the height and the width of both relativistic structures.

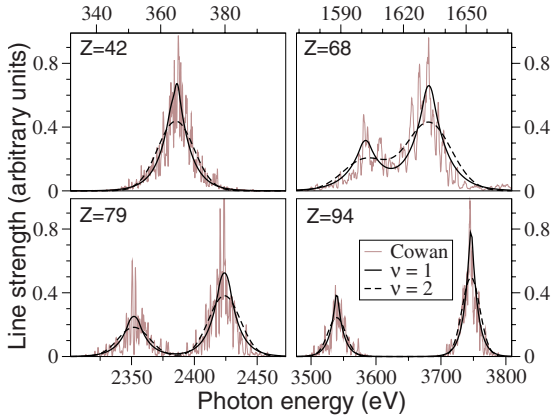

FIG. 6. (Color online) Influence of spin-orbit interactions on the 3245 lines of the isoelectronic sequence $3d^5$-$3d^4 4p$, varying the atomic number Z. The exact line-by-line calculation (light curve) is compared to statistical profiles assuming either a Gaussian (dashed line) or a Laplacian (full line) distribution. The spectra are smoothed with a resolution $\lambda/\delta\lambda=2000$.

IV. APPLICATIONS TO PHOTOABSORPTION IN HOT PLASMAS

A. Implementation of the GG functions in an atomic structure code

Usually, line broadening effects are associated to either a Gaussian profile (Doppler, instrumental width) or a Lorentzian profile (natural width, electron collisions). The line shape associated to the ionic Stark broadening is often more complex to determine, since it depends on the electrostatic field generated by the neighbor ion perturbers which splits the magnetic components of the levels and thus of the lines. However, if the number levels is high (so that the other broadening processes fill in the gap between the lines) and the matter density sufficiently weak, then the influence of the ion broadening can be accounted for roughly as an additional Gaussian width. The convolution of the Gaussian and Lorentzian profiles gives a Voigt profile

$$V(v_g,a;E)=\frac{1}{\sqrt{2\pi v_g}}K\left(\frac{E}{\sqrt{2v_g}},\frac{a}{\sqrt{2v_g}}\right), \tag{17}$$

where v_g is the sum of the variances of the Gaussian processes, a is the sum of the half-widths of the Lorentzian mechanisms, and $K(x,y)$ is the Voigt function defined by

$$K(x,y)=\frac{y}{\pi}\int_{-\infty}^{+\infty}\frac{e^{-t^2}}{y^2+(x-t)^2}dt. \tag{18}$$

In practice, we compute $K(x,y)$ using the efficient numerical algorithm proposed by Avrett and Loeser [18].

Under the assumption that $A(E)$ is Gaussian, the resulting distribution is a Voigt profile given by

$$I(E)=\Omega V(v_g+\sigma^2,a;E-\mu_1), \tag{19}$$

where Ω, μ_1, and σ^2 are, respectively, the area, the center of gravity, and the variance of the UTA.

In order to study the effects of the departure from normality, it is proposed to replace the distribution $A(E)$ by a GG function, where ν is considered as a free parameter. The resulting distribution $I(E)$ is now a cumbersome convolution of a Voigt profile by a GG function. In order to ease the implementation of the GG function in codes using Voigt profiles, it is proposed to use a mixture of Gaussian functions, which parameters (weights and variances) are obtained by a least-square fitting procedure. It was found that a fit with only five Gaussian functions is sufficient to represent a GG function with a high accuracy,

$$\frac{e^{-|u/\lambda|^\nu}}{2\lambda\Gamma\left(1+\frac{1}{\nu}\right)}\approx\sum_{k=1}^{5}\frac{a_k}{\sqrt{2\pi b_k}}e^{-u^2/2b_k}. \tag{20}$$

The ten parameters of the fit for several values of ν can be found in Table IV. This fitting method greatly simplifies the introduction of GG functions in the code, since the final distribution $I(E)$ is now a simple sum of five Voigt profiles:

TABLE IV. Parameters in Eq. (20) used to represent a generalized Gaussian function ($1 \leq \nu \leq 2$) on a Gaussian basis.

ν	a_1	a_2	a_3	a_4	a_5	b_1	b_2	b_3	b_4	b_5
1.0	0.442821	0.323849	0.183516	0.042572	0.005586	0.570341	2.094030	0.129275	0.021190	0.001710
1.1	0.452303	0.331216	0.173536	0.037290	0.004622	0.620088	2.007610	0.153826	0.027338	0.002444
1.2	0.459388	0.343772	0.160700	0.031784	0.003714	0.657210	1.898470	0.176443	0.033568	0.003269
1.3	0.463024	0.362177	0.145205	0.026302	0.002898	0.683933	1.778810	0.196913	0.039704	0.004165
1.4	0.461663	0.387640	0.127244	0.021026	0.002188	0.702256	1.656170	0.215111	0.045586	0.005107
1.5	0.452979	0.422090	0.107100	0.016103	0.001586	0.713967	1.535100	0.230950	0.051071	0.006069
1.6	0.433339	0.468627	0.085212	0.011651	0.001091	0.720667	1.418120	0.244329	0.056026	0.007024
1.7	0.396770	0.532468	0.062264	0.007763	0.000693	0.723820	1.306410	0.255050	0.060317	0.007943
1.8	0.332642	0.623153	0.039297	0.004503	0.000386	0.724887	1.200170	0.262712	0.063794	0.008792
1.9	0.219339	0.760741	0.017845	0.001910	0.000158	0.725617	1.098710	0.266538	0.066257	0.009530
2.0	0.000000	1.000000	0.000000	0.000000	0.000000	0.726079	1.000000	0.268193	0.069581	0.011245

$$I(E) = \Omega \sum_{k=1}^{5} a_k V(v_g + \sigma^2 b_k, a; E - \mu_1), \tag{21}$$

avoiding in that way any numerical convolution. The choice of a particular GG function is done by the appropriate set of parameters $\{a_k\}$ and $\{b_k\}$. It can be noticed that the fitting parameters have been given in such a way that they can be interpolated between two consecutive rows in Table IV.

B. Comparisons with experiments

Several experiments devoted to the *L*-shell spectroscopy of mid-Z elements have been published recently [19–22]. These data allow one to study the spin-orbit splitting and the effects of configuration interaction on the $n=2$ to 3 (especially $2p$-$3d$) transitions. An analysis of these experiments is proposed in order to test the new statistical modeling of the transition arrays.

1. Iron experiment

The absorption of the $2p$-$3d$ transitions of iron has been measured by Chenais-Popovics *et al.* [19] in the range 16.4–17.2 Å. The iron sample was radiatively heated by the thermal radiation of a gold spherical hohlraum irradiated by the high-power laser ASTERIX IV. The iron plasma is assumed to be in local thermodynamic equilibrium (LTE) at a temperature $T=20$ eV and a density $\rho=0.004$ g/cm^3. A simulation of this experiment using a detailed configuration accounting (DCA) approach, based on the SCO code [23], is presented in Fig. 7. It can be noticed that the departure from the Gaussian assumption allows one to better reproduce the depth of the successive oscillations in the spectrum which are due to the one-electron transitions $2p_{1/2}$-$3d_{3/2}$, $2p_{3/2}$-$3d_{3/2}$, and $2p_{3/2}$-$3d_{5/2}$ in several ion charge states.

2. Germanium experiment

An *L*-shell absorption measurement of germanium was performed in the last decade by Bruneau *et al.* [21] at the Phébus laser facility of the Centre d'Etudes de Limeil-Valenton. A germanium plasma in LTE, produced by the x rays of a laser-irradiated gold hohlraum, was probed by a short praseodymium (Pr) backlighter source using a point-projection spectrometer. The transmission spectrum that was measured in the 8–11 Å range with a resolution equal to 2.5 eV is shown in Fig. 8. The main absorption features that can be observed are the deep and wide $2p$–$3d$ transitions around 9.7 Å, the $2s$-$3p$ at 9 Å, and the $2p$-$4d$ in the range 8–8.5 Å. It can be noticed that the spin-orbit interactions are almost large enough to separate the contributions of the $2p_{1/2}$-$3d_{3/2}$ and $2p_{3/2}$-$3d_{5/2}$ transitions (the third contribution $2p_{3/2}$-$3d_{3/2}$ is negligible). The plasma conditions were determined by hydroradiative simulations to be $T=58$ eV and $\rho=0.013$ g/cm^3. The calculations were performed with a DCA code including orbital relaxation and effects of configuration interaction between semirelativistic configurations [13], which were shown to be crucial in that experiment [20]. The dashed curve in Fig. 8 corresponds to the usual Gaussian modeling of the transition arrays, whereas the full line is obtained with a GG function assuming $\nu=1$. The departure from a Gaussian profile has two main consequences. First, the calculation using the GG function reveals some struc-

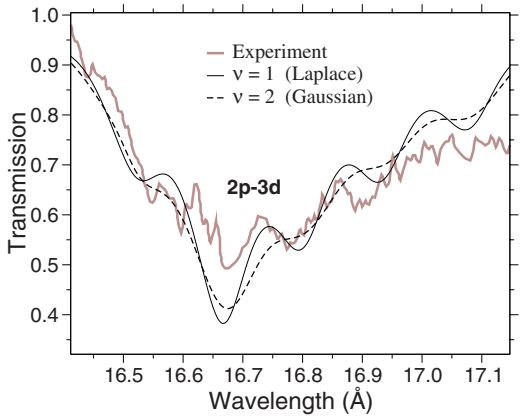

FIG. 7. (Color online) Absorption spectrum of iron measured by Chenais-Popovics *et al.* [19]. The DCA calculations are performed at $T=20$ eV and $\rho=0.004$ g/cm^3 assuming either a Gaussian (dashed line) or a Laplace (full line) distribution for the statistical UTA broadening, and using the new profile given by Eq. (21).

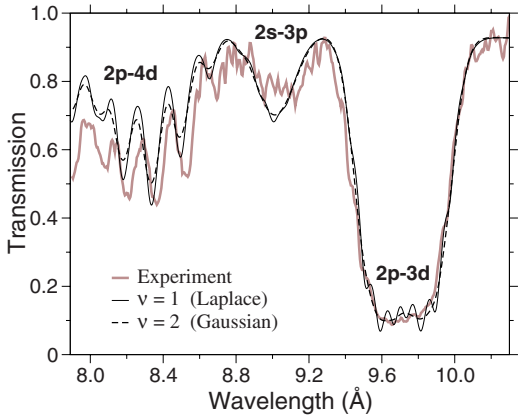

FIG. 8. (Color online) Same as Fig. 7 for the germanium experiment of Bruneau *et al.* [21] at $T=58$ eV and $\rho=0.013$ g/cm^3.

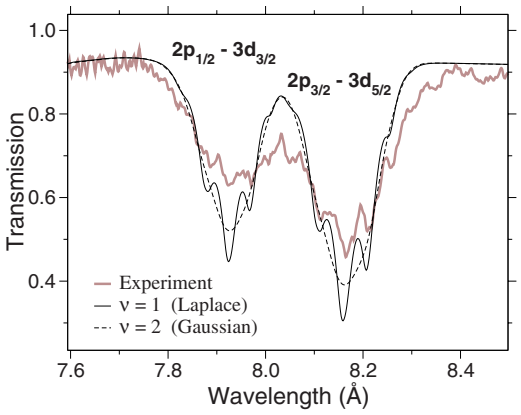

FIG. 9. (Color online) Same as Fig. 7 for the NaBr (in the Br range) experiment of Bailey *et al.* [22] at $T=47$ eV and $\rho=0.04$ g/cm^3.

tures that were not visible with a Gaussian, and which are slightly discernible in the experiment. This is clear by observing the $2p$-$3d$ transitions. Second, this increases significantly the amplitude of the oscillations of the $2p$-$4d$ transitions toward a better agreement with the experimental data. The fact that the $2p$-$3d$ transitions simulated with the Laplace distribution are slightly more resolved than observed experimentally may indicate the following: these structures are better characterized with an intermediate value $1<\nu<2$; the experimental resolution of 2.5 eV has been slightly underestimated; or this is an effect of the temperature and density gradients [20].

3. Sodium-bromine experiment

The Z pinch at Sandia National Laboratory is a very strong and bright x-ray source that enables one to efficiently heat and probe samples close to LTE. It was used by Bailey *et al.* [22] to measure absorption of CH-tamped NaBr samples. The main purpose of the experiment was to study the $2p$-$3d$ transitions in bromine ionized into the M shell. The range of sodium lines is well separated from the range of bromine lines. Electron temperature and density, obtained from the analysis of the sodium lines, are, respectively, $50(\pm 4)$ eV and $3(\pm 1)10^{21}$ cm^{-3}. The spectral resolution is about 1.5 eV. The spin-orbit interactions are now strong enough to clearly separate the $2p_{1/2}$-$3d_{3/2}$ and $2p_{3/2}$-$3d_{5/2}$ substructures. Figure 9 displays the experimental spectrum and the calculated DCA spectra at $T=47$ eV obtained with a Gaussian (dashed curve) or a GG ($\nu=1$) function (full line) for the shape of the transition arrays. Some details of the $2p$-$3d$ structures, hidden in the Gaussian description, appear clearly in the modeling and give a remarkable agreement with the experiment. This provides not only a better identification of the experimental features, but also a possible refinement of the temperature and density diagnostic.

V. CONCLUSION

The Gaussian function is widely used for the statistical modeling of complex spectra. However, to our knowledge, the effects of the departure from normality on photoabsorption calculations using the UTA approach have never been investigated. In this paper, it is shown that the Gaussian is not the most suitable distribution, and may lead to large discrepancies in the tails and the widths of the simulated spectra. This is due to the high-order moments, especially the fourth one (or kurtosis), which play a major role in the shape of the transition arrays.

We suggested, for symmetrical spectra, to function GG function, with the parameter ν constrained by the kurtosis value. Indeed, it was shown that the GG function gives an overall better agreement with the exact line-by-line calculations that cannot be achieved with a Gaussian. Since the calculation of the fourth-order moment of each transition array is very cumbersome [5], the value of the kurtosis must be fixed as an average. It is worth mentioning that this was already the case when using a Gaussian, since this is equivalent to set the kurtosis always equal to 3. In this paper, the effects of choosing another constant value for the kurtosis was investigated. It was found that it is appropriate when a limited spectral range with similar one-electron transitions is considered. This has been confirmed by the very good agreement obtained for the $2p$-$3d$ transitions of some recent experiments with calculations including non-Gaussian distributions. Moreover, the ability to increase (even excessively) the value of the kurtosis proved to be a valuable tool for the identification of the structures in the experiment and a pathway to a better estimation of the density and temperature diagnostic. As a general trend, it seems to us that the Laplace distribution ($\nu=1$) plays a privileged role in the modeling of unresolved transition arrays. The reason for this behavior is still under investigation.

A numerical fit of the GG functions on a Gaussian basis was proposed to simplify the implementation of the profile in the atomic structure codes using the Voigt function. It is interesting to mention that our fit can be used also in the superconfiguration approach [24], since super transition arrays (STA) are weighted averages of transition arrays over orbital populations. Indeed, the choice of a statistical representation beyond the Gaussian remains an issue even for the STA.

ACKNOWLEDGMENTS

We would like to thank the experimentalists, especially J. Bailey, J. Bruneau, C. Chenais-Popovics, and S. Gary for providing us the experimental data.

APPENDIX: CORRECTIONS TO THE MOMENTS DUE TO THE $(E_{ab})^p$ FACTOR

The exact n-order moment of the distribution $A(E)$ which accounts for the $(E_{ab})^p$ factor reads

$$\tilde{\mu}_n(A) = \frac{\sum_{ab} S_{ab}(E_{ab})^{n+p}}{\sum_{ab} S_{ab}(E_{ab})^p} = \frac{\mu_{n+p}(A)}{\mu_p(A)}, \tag{A1}$$

where $\mu_n(A)$ is calculated using Eq. (7).

The approximation $\tilde{\mu}_n(A) \approx \mu_n(A)$ (third UTA assumption) can be checked by considering the opacity coefficient $(p=1)$. One has for the center of gravity

$$\tilde{\mu}_1 = \frac{\mu_2}{\mu_1} = \mu_1 \left[1 + \left(\frac{\sigma}{\mu_1} \right)^2 \right], \tag{A2}$$

with $\sigma^2 = \mu_2 - (\mu_1)^2$. For the variance, one has

$$\tilde{\sigma}^2 = \tilde{\mu}_2 - (\tilde{\mu}_1)^2 = \frac{\mu_3}{\mu_1} - \left(\frac{\mu_2}{\mu_1} \right)^2, \tag{A3}$$

which can be written

$$\tilde{\sigma}^2 = \sigma^2 \left[1 + \left(\frac{\sigma}{\mu_1} \right) \alpha_3 - \left(\frac{\sigma}{\mu_1} \right)^2 \right] \tag{A4}$$

by introducing the skewness factor α_3 of the strength-weighted line energies. Therefore, the approximation is fair for $\sigma \ll \mu_1$, which is usually the case, and for near-symmetrical transition arrays.

[1] M. G. Kendall and A. Stuart, *Advanced Theory of Statistics* (Hafner, New York, 1969), Vol. 1.
[2] S. D. Bloom and A. Goldberg, Phys. Rev. A **34**, 2865 (1986).
[3] C. Bauche-Arnoult, J. Bauche, and M. Klapisch, Phys. Rev. A **20**, 2424 (1979).
[4] C. Bauche-Arnoult, J. Bauche, and M. Klapisch, Phys. Rev. A **30**, 3026 (1984).
[5] R. Karazija, Litov. Fiz. Sb. **29**, 131 (1989).
[6] M. L. Mehta, *Random Matrices and the Statistical Theory of Energy Levels* (Academic Press, New York, 1967).
[7] C. E. Porter, *Statistical Theories of Spectra: Fluctuations* (Academic Press, New York, 1965).
[8] B. G. Wilson, F. Rogers, and C. Iglesias, Phys. Rev. A **37**, 2695 (1988).
[9] R. D. Cowan, *The Theory of Atomic Structure and Spectra* (University of California, Berkeley, 1981).
[10] J. Bauche and C. Bauche-Arnoult, in *Laser Interactions with Atoms, Solids, and Plasmas*, edited by R. M. More (Plenum Press, New York, 1994), pp. 325–355.
[11] C. Bauche-Arnoult, J. Bauche, J.-F. Wyart, and K. B. Fournier, J. Quant. Spectrosc. Radiat. Transf. **65**, 57 (2000).
[12] C. Bauche-Arnoult, J. Bauche, and M. Klapisch, Phys. Rev. A **31**, 2248 (1985).
[13] F. Gilleron, J. Bauche, and C. Bauche-Arnoult, J. Phys. B **40**, 3057 (2007).
[14] J. Bauche, C. Bauche-Arnoult, and M. Klapisch, J. Phys. B **24**, 1 (1991).
[15] B. R. Judd, *Second Quantization and Atomic Spectroscopy* (Johns Hopkins University, Baltimore, 1967).
[16] C. Bauche-Arnoult, J. Bauche, and M. Klapisch, Phys. Rev. A **25**, 2641 (1982).
[17] J. Bauche, C. Bauche-Arnoult, and M. Klapisch, Adv. At. Mol. Phys. **23**, 131 (1988).
[18] E. H. Avrett and R. Loeser, Smithsonian Astrophysical Observatory Tech. Report No. 303, 1969 (unpublished).
[19] C. Chenais-Popovics *et al.*, Astrophys. J., Suppl. Ser. **127**, 275 (2000).
[20] P. Renaudin, C. Blancard, J. Bruneau, G. Faussurier, J.-E. Fuchs, and S. Gary, J. Quant. Spectrosc. Radiat. Transf. **99**, 511 (2006).
[21] J. Bruneau, S. Gary, P. Renaudin, D. Desenne, C. Blancard, P. Dallot, and G. Faussurier, Symposium Science on Large Lasers, Saclay, 1997 (unpublished).
[22] J. E. Bailey, P. Arnault, T. Blenski, G. Dejonghe, O. Peyrusse, J. J. MacFarlane, R. C. Mancini, M. E. Cuneo, D. S. Nielsen, and G. A. Rochau, J. Quant. Spectrosc. Radiat. Transf. **81**, 31 (2003).
[23] T. Blenski, A. Grimaldi, and F. Perrot, J. Quant. Spectrosc. Radiat. Transf. **65**, 91 (2000).
[24] A. Bar-Shalom, J. Oreg, W. H. Goldstein, D. Shvarts, and A. Zigler, Phys. Rev. A **40**, 3183 (1989).